J. Mt. Sci. (2019) 16(5): 1035-1047 e-mail: jms@imde.ac.cn http://jms.imde.ac.cn
https://doi.org/10.1007/s11629-018-5289-3

Quantitative analysis of the macro-geomorphic evolution of Buyuan Basin, China

GU Zhen-kui[1,2] https://orcid.org/0000-0002-5023-7431; e-mail: bygzk853@126.com

FAN Hui[1,2*] https://orcid.org/0000-0002-6069-5145; e-mail: fanhui@ynu.edu.cn

SONG Zhao-jun[3] https://orcid.org/0000-0001-6516-2818; e-mail: songzhaojun76@163.com

**Corresponding author*

1 Yunnan Key Laboratory of International Rivers and Transboundary Eco-Security, Yunnan University, Kunming 650091, China

2 Institute of International Rivers and Eco-Security, Yunnan University, Kunming 650091, China

3 Shandong Provincial Key Laboratory of Depositional Mineralization & Sedimentary Minerals, College of Earth Science and Engineering, Shandong University of Science and Technology, Qingdao 266590, China

Citation: Gu ZK, Fan H, Song ZJ (2019) Quantitative analysis of the macro-geomorphic evolution of Buyuan Basin, China. Journal of Mountain Science 16(5). https://doi.org/10.1007s11629-018-5289-3

Abstract: Buyuan River, the largest tributary within the Chinese Lancang-Mekong River region downstream of the Jinghong Dam, plays a crucial role in river function and ecosystem service of the Lancang-Mekong River. The geomorphic evolution of a basin exerts a key control on riverine sediment input and transport. In this study, the geomorphic characteristics of Buyuan Basin are analyzed using morphological parameters, hydrodynamic parameters and the stream power river incision model. The results show that: 1) The slight north-south difference of channel density is most likely due to lithology and independent of tectonic activity and climate. 2) The weak tectonic activity and the low hypsometric integral (*HI*) value suggest that the macroscopic landform condition limits erosion and sediment production. 3) The logarithmic longitudinal profile of the main channel defends that the upstream sediments generated by erosion are easily deposited in the downstream channel, rather than being transported directly into the Lancang-Mekong River. 4) Approximately 74% of the reaches have annual average stream power less than 500 $W \cdot m^{-1}$. The narrow variation ranges of stream power in 50% of the river channel indicate relatively stable hydrodynamic environment. 5) Stream erosion and tectonic activity make the longitudinal profiles of the main channel and most tributary channels unstable. The wide range (between 22.01 and 45.58 with θ=0.43) of steepness index (k_{sn}) of longitudinal profiles implies differential uplift in the basin.

Keywords: Geomorphic parameters; Steepness index; Stream power; Lancang-Mekong River

Received: 09-Nov-2018
1st Revision: 02-Jan-2019
2nd Revision: 31-Jan-2019
Accepted: 17-Feb-2019

Introduction

A basin is a natural hydrological entity that allows surface runoff to a defined channel, drain, stream, or river at a particular point (Chopra et al. 2005). The geomorphic evolution of basin is an important aspect of land surface change, reflecting variations in the coupling system of tectonic activity-landform-climate (Wang et al. 2017; Du et al. 2018; Li et al. 2018). There is a close relationship between surface morphology change,

sediment yield, and the sediment transport capacity of a river (Singh et al. 2008; Zhang et al. 2015). Using geomorphic features, it is possible to indirectly interpret the dynamic characteristics and driving mechanisms of the surface environment. Common geomorphological parameters include the hypermetric integral (Stucki and Schlunegger 2013), drainage basin asymmetry factor (Owono et al. 2016), and stream length-gradient index (Owono et al. 2016). These parameters are often used to understand the characteristics of tectonic activity in large-scale basins (Mahmood and Gloaguen 2012; Gao et al. 2013; Wu et al. 2014). Moreover, over more than a decade, the stream-power river incision model has been greatly developed and our understanding of the evolution mechanism of longitudinal profiles has correspondingly improved, compensating for the lack of geomorphic evolution analysis by simple morphological measurement (Perron and Royden 2013; Wang et al. 2017). However, the stream-power river incision model is based on the empirical function of the discharge and catchment area, and the model does not directly introduce modern precipitation and discharge information, so cannot easily reflect spatial variation of the erosion dynamic environment. To enhance our understanding of geomorphic features, more attention should be paid to the mechanism of morphological and hydrodynamic changes in river environments.

At present, geoscientific research into global basins is becoming increasingly urgent due to accelerated global integration (Bernauer 2002; He et al. 2004; Alekseevskii et al. 2015). Despite being the most well-known international river in Southeast Asia, the Lancang-Mekong River, which begins in the Tibetan Plateau, is still not fully understood. Some recent studies have focused on the geomorphic features of its large fluvial system, such as reconstruction of paleoaltimetry and the ancient erosion rate (Hoke et al. 2014; Zhang et al. 2018); however, research remains fairly limited. To date, no studies on the macro-geomorphic features of Lancang-Mekong tributaries have been conducted. The Buyuan River, an important tributary of the Lancang-Mekong River, is an important fish migration protection area (Fan et al. 2015). Sediment yield and sediment transport in this basin directly affect the transboundary ecological security, and the macroscale geomorphological features fundamentally determine the potential of sediment yield (Zhang et al. 2015). Therefore, by calculating the geomorphic parameters, analyzing the characteristics of the stream-power river incision model, and estimating stream power values, we perform a comprehensive evaluation of the macroscopic geomorphic features in the Buyuan River basin. This research is beneficial for understanding geomorphic evolution mechanisms and identifying major sand production areas, thereby providing a reference for formulating management measures and further exploring the relationship between the main stream of Lancang-Mekong River and its tributaries.

1 Methodology

1.1 Study area

Buyuan Basin (Figure 1), located in China, comprises an area of approximately 8931 km^2 with an elevation of 500-2290 m, formed during the uplift of Qinghai-Tibet Plateau in Cenozoic. In the early Paleozoic period, the basin was an interactive zone of coastal continental erosion and transgression. In the late Paleozoic, it was in a marine environment, forming limestone and dolomite strata. Since the early Mesozoic period, the basin has evolved into a continental environment with sandstone and mudstone as the main strata (Li et al. 1982). The basin is located in the south of Simao block, where the Indian Plate has pushed into the Asian plate and caused strong deformation. The larger faults in the basin have a north-south strike. Most faults are strike-slip faults, some of which are normal faults with a strike-slip rate of 0.2-4 mm·yr^{-1} and the main fault activities started from the Pliocene epoch (Wu 2016). Sedimentary layers formed during the Mesozoic period are similar but the formation periods are different; Lower Cretaceous strata is observed in the north, whereas strata in the south are older, with the most southern area exhibiting older late Paleozoic strata (Figure 1). The basin is affected by a subtropical monsoon climate. The average annual temperature and precipitation values are approximately 21.5°C and 1488 mm, respectively,

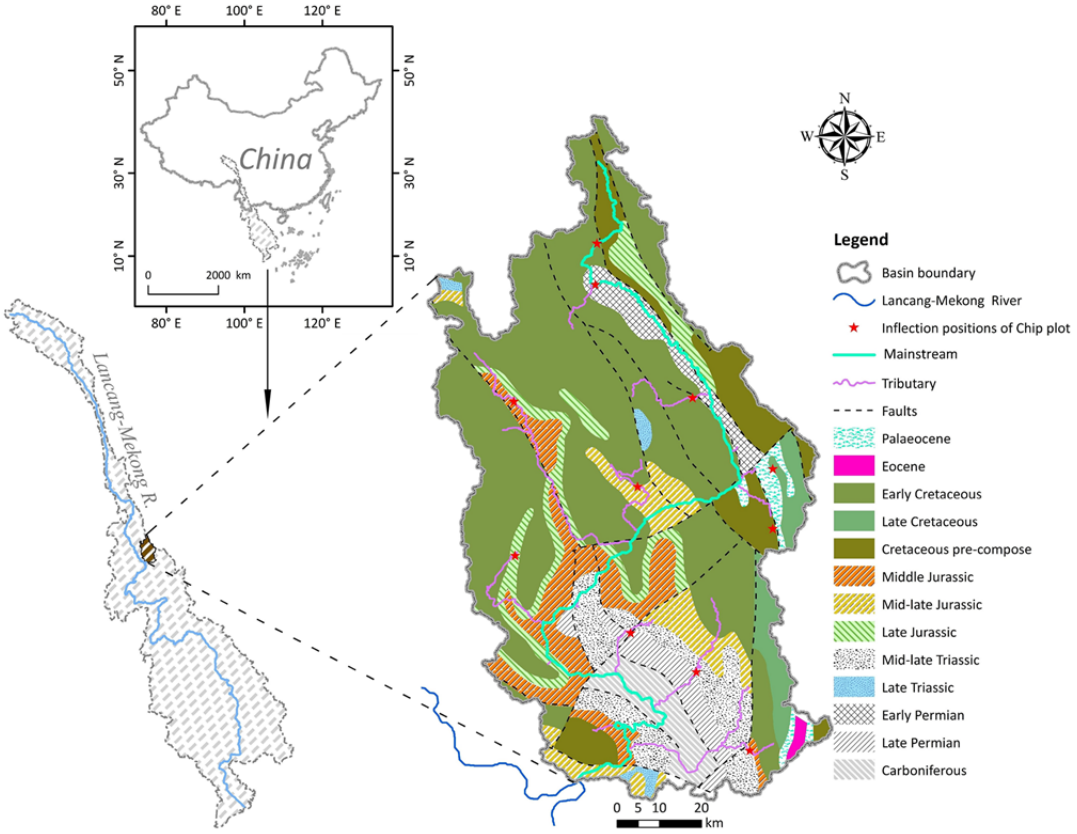

Figure 1 Geological Map of Yunnan Province (scale 1:2500,000, Ma 2002) showing the study area within 21.78°-23.14°N, and 100.86°-101.69° E. Inflection positions in this diagram indicate where the χ-z lines are significantly bent when calculating steep indexes by the integral approach (Perron and Royden 2013).

the latter of which is mainly concentrated from June to November each year. Stream discharge is mainly recharged by precipitation and varies seasonally. The average annual runoff is 178.1 $m^3 \cdot s^{-1}$, accounting for 1.19% of the discharge of Lancang-Mekong River into the sea. Influenced by runoff, river sediment transport is also mainly concentrated in the flood season from June to November, with an average annual sediment transport volume of approximately 5.2953 $Mt \cdot yr^{-1}$ (Zhong et al. 2011). The Basin plays a crucial role in river function and ecosystem service of the Lancang-Mekong River because fish from lower Lancang-Mekong will follow the Buyuan River upstream in the fish migration season. Besides, it belongs to the basin with good vegetation coverage, and the species of animals and plants are relatively rich.

1.2 Data

The data used in this research mainly include: 1) the Geological Map of Yunnan Province (scale 1:2500,000, Ma 2002); 2) an SRTM 1 Arc-second DEM (http://earthexplorer.usgs.gov) with an absolute elevation error of approximately 4 m (Chen et al. 2012; Pipaud et al. 2015; Rabah et al. 2017; Wu et al. 2017); 3) rainfall data (https://www.ecmwf.int/); and 4) average discharge data recorded at hydrologic stations (Zhong et al. 2011).

1.3 Methods

Geomorphologic analysis includes both qualitative and quantitative approaches, all of which are based on the principle that any bedrock deformation or lithologic variation has a morphological signature (Owono et al. 2016). Relevant morphological parameters for analyzing the topographic features of a basin include the channel density (C_d), hypsometric integral (*HI*), drainage basin asymmetry factor (*AF*), index of drainage basin shape (*Bs*), and stream length-

gradient index (*SL*). In addition, the evolution stage of the longitudinal profile is reflected by functional morphological fitting (Rãdoane et al. 2003). Stream Power (*Ω*) and the gradient of stream power (*GSP*) are used to reflect the increase and decrease in the strength of hydraulic action (Table 1).

1.3.1 Evaluation of relative tectonic activity

Evaluations of relative tectonic activity using geomorphological features typically rely on *IRAT* values (index of relative active tectonics) by assigning values to intervals in which the geomorphic parameters are located, then averaging the value as *IRAT* (Mahmood and Gloguen 2012). This is an imprecise method of evaluation. However, with higher *HI*, *AF*, *SL/K*, and *Bs*, which indicates stronger tectonic activity, the calculation method of *IRAT* is changed slightly to reduce the error caused by the artificial assignment process:

$$NIRAT = \frac{S_{HI}+S_{AF}+S_{SL/K}+S_{Bs}}{4} \quad (1)$$

where S_{HI}, S_{AF}, $S_{SL/K}$, and S_{Bs} are the normalized results of *HI*, *AF*, *SL/K*, and *Bs* series values. Therefore, the larger the *NIRAT* value, the stronger the tectonic activity.

1.3.2 Coupling characteristics of internal and external forces

Bedrock channels are subject to stream erosion and tectonic activity. When the hydraulic undercut rate (*E*) and uplift rate (*U*) are equal in the bedrock channel, channel elevation does not change with time; i.e.,

$$U(x,t) = KA^m(\frac{\partial z}{\partial x})^n \quad (2)$$

where *K*, *z*, *x*, and *t* represent erosion coefficient, the channel elevation, distance, and time, respectively, and $k_{sn}=(U/K)^{1/n}$ is the steepness index, which is used to indicate the uplift rate of

Table 1 Formulas and interpretations of the morphological parameters used in this study.

Parameters	Formulas	Interpretations
C_d	$C_d=(\sum L)/A$ $\sum L$, total length of river channel in the basin; *A*, basin area (Dar et al. 2014).	A larger channel density equals a more fragmented surface and a greater degree of erosion.
HI	$HI=(H_{mean}-H_{min})/(H_{max}-H_{min})$ H_{mean}, H_{max}, and H_{min} denote the mean, maximum, and minimum heights of a basin, respectively (Pike and Wilson 1971).	*HI*> 0.7, 0.5 ≤*HI* ≤0.7, and *HI* <0.5 equate to high, moderate, and low levels of tectonic activity, respectively (Altın 2012; Mahmood and Gloaguen 2012).
AF	$AF = 100\times(Ar/At)$ *Ar* denotes the area of the basin on the right side of the trunk stream, while *At* refers to the total basin area.	|*AF*-50| > 15, 7 ≤| *AF*-50| ≤ 15, and |*AF*-50| < 7 equate to high, moderate, and low levels of tectonic activity, respectively (Gao et al. 2013; Gao et al. 2016).
SL	$SL = (\Delta H/\Delta L)\cdot L$ ΔH denotes the difference in elevation between the ends of the river reach under consideration, ΔL denotes the length of the reach, and *L* is the distance between the measured reach and the drainage divide.	*SL*/*K* ≤ 2 = gentle reach, reflecting weak tectonic activity; 2<*SL*/*K* ≤10 = steep, reflecting strong tectonic activity; *SL*/*K* > 10 = extremely steep reach, strong tectonic activity. *SL*/*K* = normalized stream-length gradient index without the effect of the mesoscale difference of *SL* (Seeber and Gornitz 1983). *K* is the slope of the line from the start point to the end point on the Hack profile.
Bs	$Bs = Bl/Bw$ *Bl* denotes the basin length measured from the headwater to the mouth, while *B*w is the maximum basin width.	High, moderate, and low levels of tectonic activity have values of *B*s > 3, 2–3, and < 2, respectively (Hamdouni et al. 2008; Gao et al. 2016).
Ω (W·m^{-1})	$\Omega=\gamma\cdot Q\cdot s$ γ is the unit weight of water per unit length (9800 N·m^{-3}), *Q* is the discharge (m^3·s^{-1}), and *s* is the slope of the water surface, which is generally approximated by the slope of the channel bed (Pérez-Peña et al. 2009).	Ω, hydrodynamic strength; *Q* can be calculated by a simple method (Gu and Shi, 2018); *s* is obtained by linear regression sliding along the longitudinal profile on a scale of 1 km.
GSP (W·m^{-2})	$GSP= \Omega/L$ *L*, the analytical scale in the calculation, is 5 km in this study.	Positive *GSP* = stream power increases downstream and the river has incision force; negative value = stream power decreases downstream and the carrying capacity of the river decreases; 0 = hydrodynamic condition is stable and erosion and deposition are balanced.

the bedrock channel, $s=\partial z/\partial x$ is the channel slope, $\theta=m/n$ is the reference concavity, and m and n are constants. The k_{sn} and θ values can be obtained by the Chi-plot (χ-z) proposed by Perron and Roden (2013), and the balance between channel uplift and erosion can be examined simultaneously using the following equations:

$$z = z_b + \left(\frac{U}{KA_0^m}\right)^{\frac{1}{n}} \chi \quad (3)$$

$$\chi = \int_{x_b}^{x} \left(\frac{A_0}{A}\right)^{m/n} dx \quad (4)$$

where z is the elevation at position x, z_b is the elevation of the datum position, x_b is the location of the datum, and A_0 is a reference area (Perron and Royden 2013; Shi and Shao 2014). The difference in reference concavity (θ) will cause the change of χ. In order to obtain an appropriate reference concavity, θ can be changed from 0 to 1 and the corresponding θ can be selected as the reference concavity when the linear fitting coefficient (R^2) of χ-z is the maximum. If there are a series of sub-basins, the average value of reference concavity is taken as the reference concavity of whole region (Perron and Royden 2013).

2 Results

2.1 Landform pattern

2.1.1 Channel density

Channel density is an important parameter for determining the level of landscape dissection due to the action of fluvial systems and is a good measure of the fineness of basin topography (Dar et al. 2014). In general, the relationship between channel density and precipitation, discharge, rock features, tectonic activity and others are typically considered in geomorphology studies (Zhao et al. 2016). In this study, different threshold values (catchment area) were extracted to determine different river channel densities. A larger threshold value leads to more abundant external force conditions of channel evolution and more obvious river characteristics. In order to analyze the spatial differences of channel density, we divided the Buyuan Basin into 20 sub-basins (Figure 2a) and calculated the channel densities corresponding to different threshold values. The relationship between catchment area value and the corresponding channel density follows an exponential function (Figure 3a). The channel densities in the northern part differ from those spatially in the southern. Average channel densities in the northern part (B1-B10) range from 0.19–0.20 km·km^{-2}, with a corresponding threshold of 9.86 km^2. Average channel densities in the southern part show a wider range, from 0.16–0.24

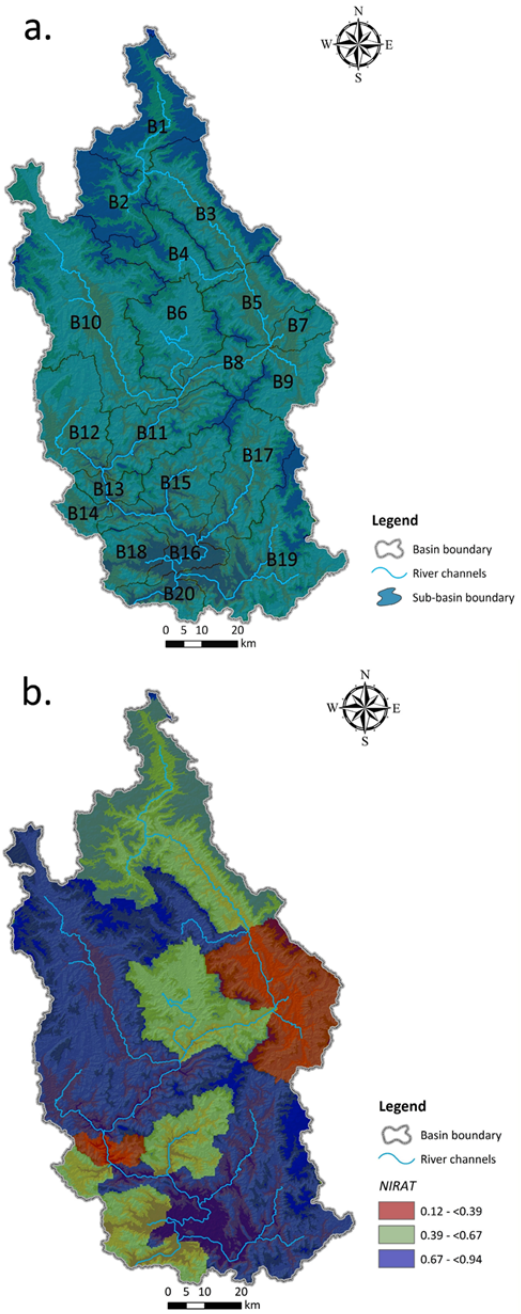

Figure 2 (a) Sub-basins of the Buyuan Basin and (b) spatial characteristics of tectonic activity intensity.

km·km^{-2}, and are generally slightly lower than those in the north (Figure 3b).

2.1.2 Characteristics of HI, AF, Average SL/K, and Bs

HI is used to reflect the relative volume of the geologic body above the erosion datum; the greater the *HI* value, the more erosion will occur. *HI* is mainly related to the erosion conditions and tectonic activity, so it can be used to reflect the difference of tectonic activity in a region with similar climatic conditions (Stucki and Schlunegger 2013). The value of *HI*, *AF*, average *SL/K* and *Bs* for the entire basin is 0.38, 55.98, 4.15 and 1.79, respectively. This low value is possibly related to older landscapes that have been more eroded and less impacted by recent active tectonics (Mahmood and Gloaguen 2012), indicating that the intensity of tectonic uplift activity in the basin is far inferior to the geomorphic conditions that encourage erosion and increased sediment yield. We also computed *HI* for each sub-basin, which indicates values between 0.28 and 0.56 (Figure 4), where most sub-basins have a *HI* value greater than 0.35. Hypsometric curves of the sub-basins can be divided into four categories: concave-convex (B1, B2, B4, B6, B9, B10, B11, B12, B14, B15, B17, and B19), concave (B16), linear hypsometric (B13), and

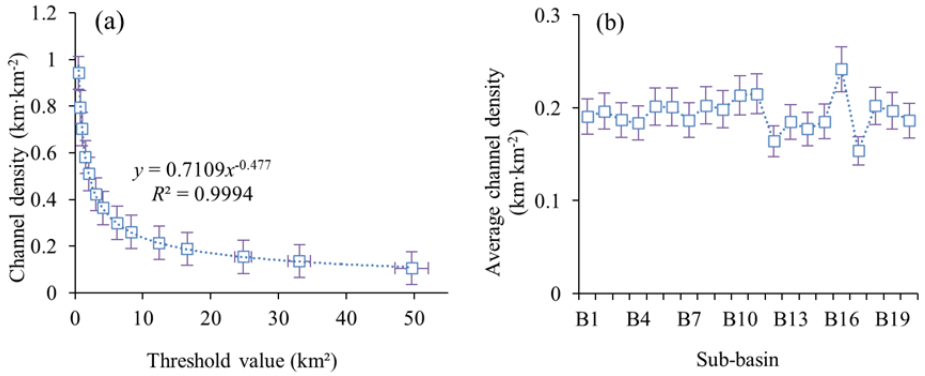

Figure 3 (a) Variations of channel density for different threshold values and (b) average channel density in different sub-basins. The yellow bar means standard deviation.

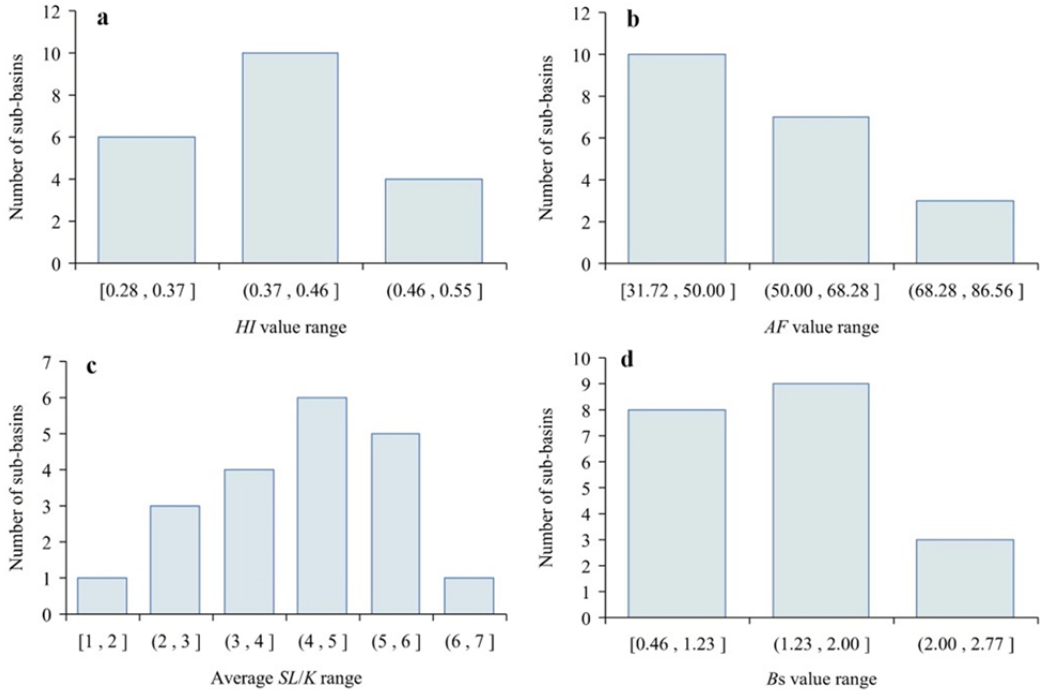

Figure 4 Distribution of tectonic geomorphic parameters by sub-basin.

concave-linear (B3, B5, B7, B8, B18, and B20). Convex curves (B2) are rare, and there are a few prominent uplift sites in the basin (Figure 5). Moreover, correlation analysis shows that the relationship between most parameters is not significant (Table 2), but there is a negative correlation between precipitation and *HI*, indicating that more rainfall leads to stronger erosion.

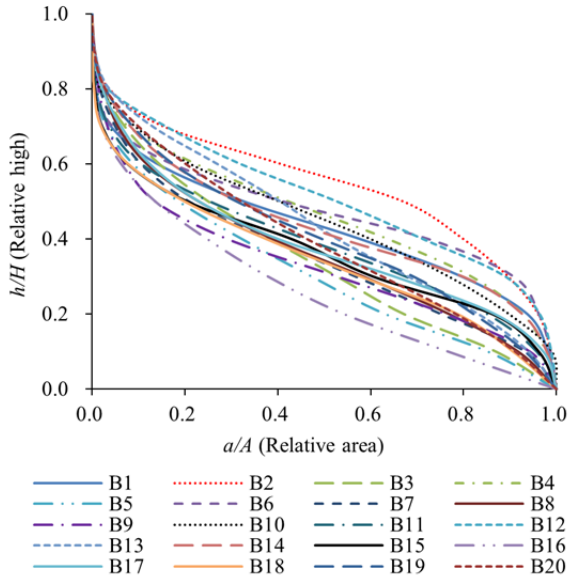

Figure 5 Hypsometric curves of each sub-basin. A = basin area; a = the area enclosed by the contour line with the height h above the elevation of the outlet position; H = maximum height difference.

AF is widely used to detect tectonic tilting transverse to flow at the basin level and is highly sensitive to tectonic activity (Dar et al. 2014). An *AF* value of 55.98 was calculated for the entire basin, indicating a slight eastward slope of the basin. The number of sub-basins with an *AF* value of less than 50 and those with an *AF* value of greater than 50 are the same in the Buyuan Basin (Figure 4), which suggests that there is little tilting perpendicular to the direction of the trunk channel. *SL*/*K* is very sensitive to the change of longitudinal profile slope and is often used to indicate local faults (Seeber and Gornitz 1983). In order to understand the overall situation of the basin, we calculated the average *SL*/*K* of the stem-channel in each sub-basin and found that most sub-basins have an average *SL*/*K* value of greater than 2 (Figure 4c), indicating rather steep channels. Additionally, the *Bs* value is 1.79, which reveals that the basin is not strongly elongated. Most of the parameters do not show a significant correlation (Table 2), which indicates that tectonic activities such as uplift and fault development are independent in each region of the basin.

2.1.3 Relative tectonic activity intensity

Geomorphic parameters are powerful tools for evaluating the influence of active tectonics (Mahmood and Gloaguen 2012). This investigation is an attempt to evaluate relatively active tectonics over a large area based on several sub-basins and using a number of geomorphic parameters. According to the calculated *NIRAT* values, areas with relatively strong tectonic activity are mainly in the north-west and south-east of the basin, while the remaining areas exhibit relatively weak activity (Figure 2b); areas with relatively strong tectonic activity account for the largest proportion of the basin (Figure 6).

Table 2 Correlation coefficients between morphological parameters.

	C_d	*HI*	|*AF*-5|	*SL*/*K*	*Bs*	Prec.
C_d	1	-0.403	-0.087	0.152	-0.033	0.000
HI		1	0.146	0.079	-0.138	-0.445*
|*AF*-50|			1	0.312	0.190	0.344
SL/*K*				1	0.124	0.315
Bs					1	-0.111
Prec.						1

Note: *, significant at α=0.05. Prec.=Precipitation

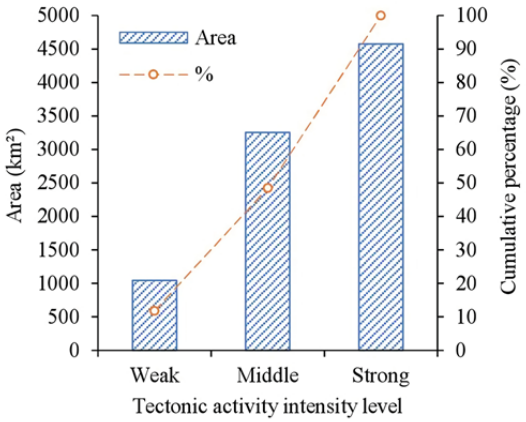

Figure 6 Area and cumulative percentage of different tectonic activity intensity zones for the whole basin. Levels are based on equal intervals of *NIRAT*.

2.2 Stream analysis

2.2.1 Evolution stage and local steep characteristics of longitudinal profile

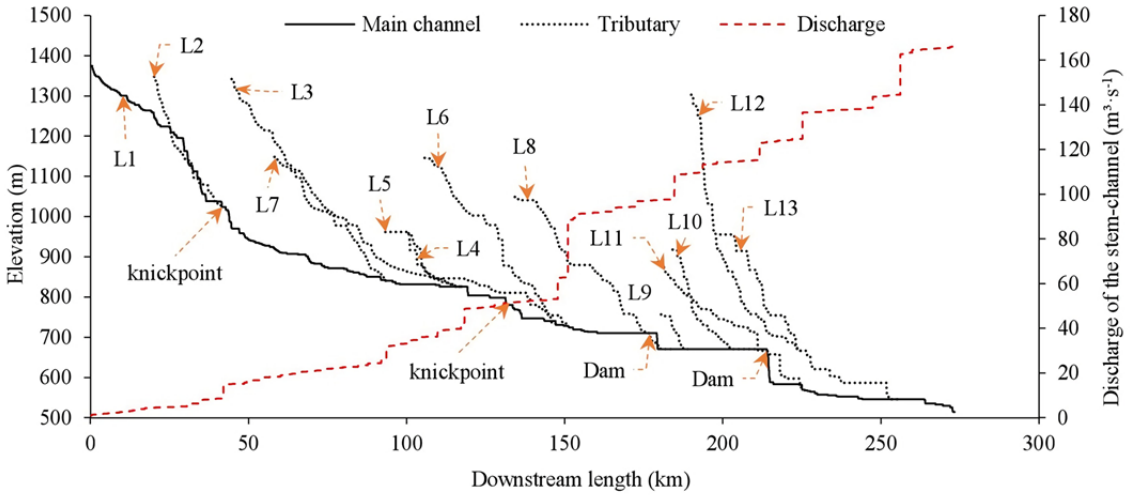

Figure 7 Longitudinal profiles with observed knickpoints marked on the mainstream channel and discharge of the main channel.

The evolution of longitudinal river profiles is related to bedrock, sediments, hydrodynamic strength, and tectonic activity (Whipple and Tucker 1999; Ambili and Narayana 2014; Zhang et al. 2015). After uplift of the basin, longitudinal profile morphology generally varies between linear, exponential, logarithmic, and exponential during the process of erosion (Ohmori 1991; Rãdoane et al. 2003). There are 13 longitudinal profiles in the basin, including the main stream and major tributaries (Figure 7). In order to determine the stage of erosion and evolution of each longitudinal profile, four simple functions were fitted to our data. The results are presented in Table 3. The best fit for the profile of the stem-channel is the logarithmic model whereas the optimal model fit for the longitudinal profile of most tributary channels is linear (Table 3). This may suggest that the longitudinal profile of the mainstream channel has undergone a more rapid evolution process than that of the tributary channels. Reaches with *SL*/*K* values greater than 2 are densely distributed in the tributary channels (Figure 8). Gentle reaches appear more often downstream of the stem-channel, with lengths of hundreds of kilometers, accounting for 43.5% of the total river length in the basin. Extremely steep reaches are rare, accounting for less than 10% of the total river length (Figure 9).

2.2.2 Characteristics of stream power and stream power gradient

Stream power indicates the sediment transport capacity of the river and is the most direct reflection of the strength of the hydrodynamic force (Summerfield 1991). The stream power in most channel reaches of the basin is less than 500 W·m^{-1}, which accounts for 74% of the total length of channels. Channel reaches with stream power between 500 and 2000 W·m^{-1} account for 19% of the total length (Figure 10a and Figure 11a). The *GSP* value for 50% of the length of all channels is close to 0, providing a more stable dynamic environment for sediment transport. When the *GSP* is negative, the stream power decreases downstream and silt is likely to be deposited; the length of negative *GSP* channels is approximately 25% and approximately equal to the length of eroded reaches (Figure 10b and Figure 11b).

Table 3 R^2 values for linear, exponential, logarithmic, and power models of each sub-basin.

Profile (sub-basin)	Linear	Exponential	Logarithmic	Power
L1*	0.8928	0.7448	0.9012**	0.4761
L2 (B2)	0.9483**	0.6052	0.8488	0.3176
L3 (B4)	0.9881**	0.7567	0.7728	0.4252
L4 (B7)	0.8128	0.8187**	0.8111	0.4848
L5 (B9)	0.9166**	0.6568	0.6575	0.3089
L6 (B6)	0.9834**	0.5556	0.7040	0.2798
L7 (B10)	0.9031**	0.6558	0.8632	0.4326
L8 (B12)	0.9834**	0.6324	0.7229	0.3058
L9 (B14)	0.9278**	0.7919	0.6329	0.4066
L10 (B15)	0.8028	0.8756*	0.8499	0.5189
L11 (B17)	0.9730**	0.6990	0.7353	0.4896
L12 (B19)	0.7749	0.7580	0.9466**	0.5063
L13 (B19)	0.9671**	0.5855	0.6790	0.3050

Note: * = longitudinal profile of the stem-channel, which flows through sub-basin B1, B3, B5, B8, B11, B13, B16 and B20; ** = best fit.

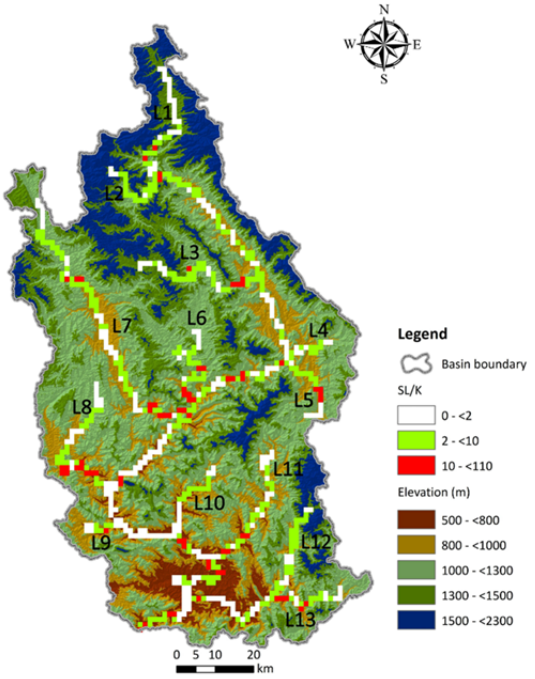

Figure 8 Distribution characteristics of the *SL*/*K* value. *SL*/*K* ≤ 2 = gentle reaches, 2 < *SL*/*K* ≤ 10 = steep reaches, and *SL* >10 = extremely steep reaches (Seeber and Gornitz 1983).

Table 4 Parameters of the stream-power river incision model (θ=0.43).

Profile (sub-basin)	k_{sn}	R^2	Steady-state
L1*	28.36	0.9725	Worse
L2 (B2)	45.58	0.9872	Better
L3 (B4)	33.27	0.9882	Better
L4 (B7)	22.01	0.8627	Worse
L5 (B9)	22.24	0.9283	Worse
L6 (B6)	44.03	0.9670	Worse
L7 (B10)	22.93	0.9726	Worse
L8 (B12)	30.45	0.9662	Worse
L9 (B14)	29.92	0.9311	Worse
L10 (B15)	31.63	0.8776	Worse
L11 (B17)	28.67	0.9613	Worse
L12 (B19)	41.74	0.8979	Worse
L13 (B19)	41.10	0.9570	Worse

Notes: *= longitudinal profile of the stem-channel through sub-basin B1, B3, B5, B8, B11, B13, B16, and B20. R^2 > 0.98 or R^2 < 0.98 indicate that the steady-state is better or worse, respectively; this classification criteria is determined subjectively by comparing the morphology of χ-z line with the R^2 value.

2.3 Coupling effect of internal and external forces

The elevation change of bedrock channel is equal to the difference between the height of crustal uplift and the height of erosion cutting. When the crustal uplift rate is equal to the river's cutting rate, the position of channel height remains unchanged, and the channel is in a stable state (Whipple and Tucker 1999). By calculating the θ value corresponding to the optimal fit and taking the average as the uniform reference concavity, we draw the χ-z lines (Figure 12a). The results show that the χ-z relationships do not reveal perfectly linear features; some features are highly curved and some almost linear features contain small amplitude bends (Figure 12a, b). If the influence of lithology is ignored, the longitudinal profile of the stem-channel and most of its tributaries are considered to be unstable. From the general situation, the k_{sn} value range of each profile is basically between 22.01–45.58, which reflects the inconsistency of uplift rate in the basin (Table 4).

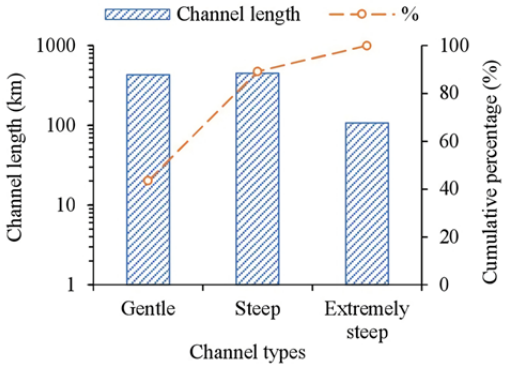

Figure 9 Length and proportion of gentle, steep, and extremely steep reaches in the basin.

3 Discussion

3.1 Lithology and channel density

The surface of Buyuan Basin is predominantly covered by Mesozoic sedimentary rocks. Uplift of the Qinghai-Tibet Plateau since the Cenozoic has transformed it from a sedimentary area into an erosive area where the basin gradually formed. Evolution of basin results from an adjustment between processes of erosion as streams and rivers flow over rocks and soils of variable strength (Hack 1973). The characteristics of channel density are closely linked to this process. According to our calculations, the river channel density in the southern part of the basin is slightly lower than that in the northern part (Figure 3b). However, we

also note that exposed strata in the southern part of the basin are relatively old, whereas the northern part is mainly covered by relatively young Cretaceous strata (Figure 1). Therefore, this may indicate an effect of lithologic differences on the channel density. In addition, channel density does not correlate to tectonic geomorphic parameters and precipitation (Table 3), and precipitation differences within the basin are relatively limited under the same climatic conditions; this implies that tectonic activity and climate have a minimal influence on channel density. In general, the higher the uplift degree of a basin, the smaller the channel density will be (Dar et al. 2014); however, higher uplifted areas in the northern part of the basin, as reflected by the hypsometric curves, have slightly higher channel density (Figure 3b), indicating that this rule is not applicable to the Buyuan Basin. Therefore, the influence of tectonic activity and climate can be disregarded, and it can be concluded that the slight difference of channel density is likely caused by spatial differences of lithology; i.e. for the same kind rock, strata in the southern part of the basin are old and may have a higher consolidation degree and slightly stronger corrosion resistance, resulting in a slightly slower development of channel density.

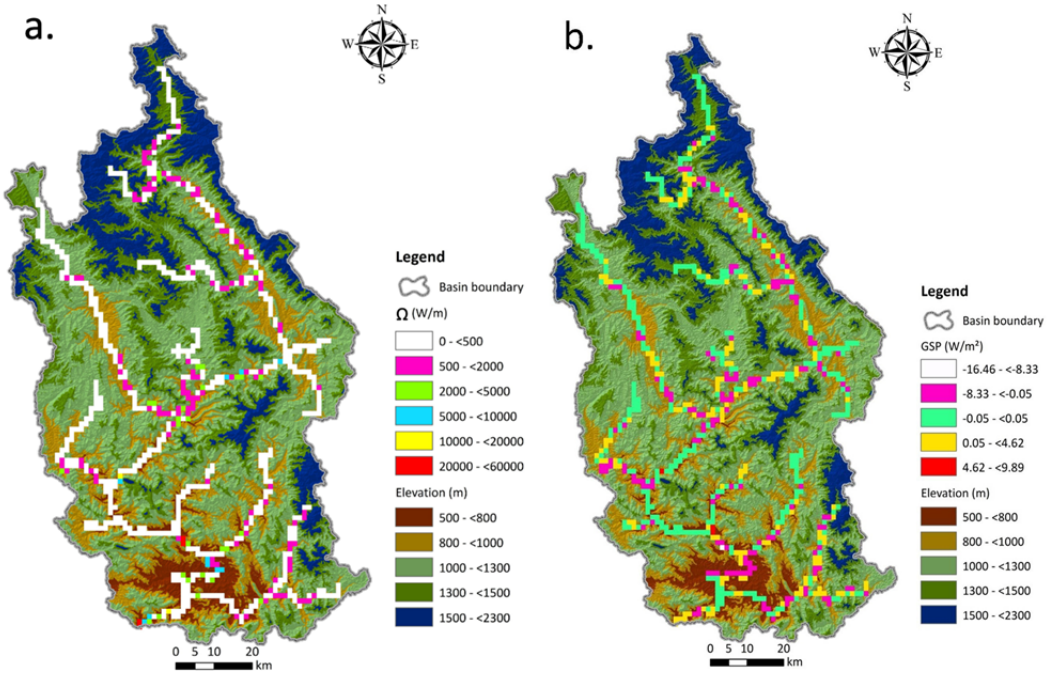

Figure 10 Characteristics of (a) stream power and (b) the gradient of stream power.

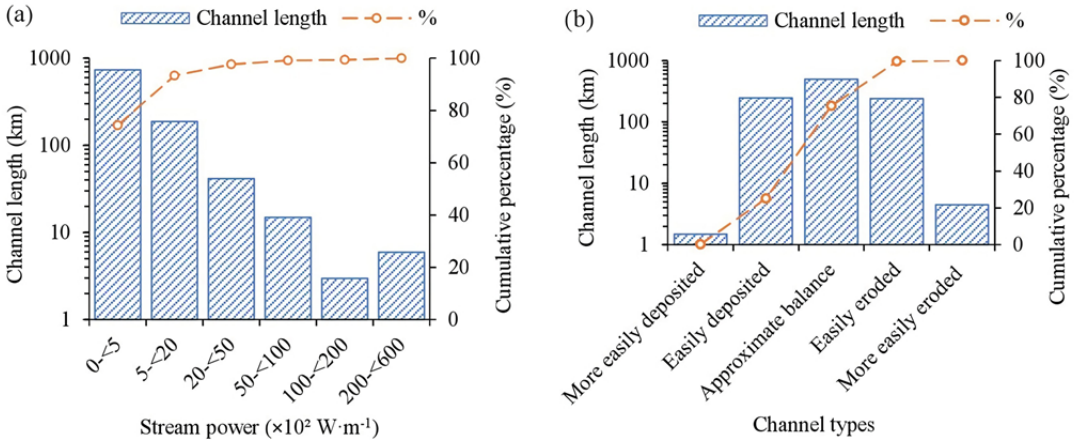

Figure 11 Lengths of channel reaches in (a) different stream power intervals and (b) erosion-deposition reaches.

3.2 Longitudinal profile evolution and sediment yield

If we look only at their morphological characteristics, the longitudinal profiles of the tributary channels are generally in the early stage of erosion. These longitudinal profiles with approximate linear characteristics are advantageous for erosion. In contrast, the longitudinal profile of the mainstream channel is logarithmic. Under the condition of this, the upstream sediments generated by erosion are easily transported to the downstream channel and deposited, rather than being injected directly into the Lancang-Mekong River. Therefore, in terms of the channel sediments, it can be concluded that the sediments entering the Lancang-Mekong River mainly come from the tributaries rather than from erosion of the mainstream channel itself. Figure 10b shows the distribution of *GSP* in the basin. Lengths of erodible and sediment-prone reaches are approximately the same. The low-value reaches of *GSP* near the estuary should be relatively easily turned into silt deposition areas, which play a role in reducing the sediment output into the Lancang-Mekong River.

3.3 Tectonic activity of the basin

According to a study of river terraces, the upper reaches of the Lancang-Mekong River experienced four stages of accumulation and subsequent down-cutting in the late Quaternary (Zhang et al. 2018). Buyuan River is a tributary of the downstream Lancang River (Figure 1), which may also have been affected by the unbalanced effects between tectonic uplift and erosion. The river incision rate near the intersection of Buyuan river and lancang River is about 0.13-0.22mm·yr^{-1} (Zhang et al. 2018). According to our results, the linear characteristics of the main stream and most of the tributaries in the Chi plot are not particularly clear. Concave parts of the χ-z line indicate that erosion rate is greater than uplift rate. However, the χ-z lines of longitudinal profiles of the stem-channel and one tributary (L12) are bent to a greater extent (Figure 12a), which is less likely to be caused by lithological differences because lithological differences within the basin are not significant. To determine whether this judgment is correct, we label inflection positions of the χ-z line on Figure 1 and find that most positions lie near the fault (Figure 1), suggesting that the fault is predominantly responsible for bending of the χ-z line. According to the integral approach, if all χ-z lines coincide, all sub-basins have the same uplift rate (Perron and Royden 2013). However, our analysis results show that k_{sn} values of longitudinal profile are different, indicating different uplift rates in different sub-basins (Table 4), which is likely a reason for the multiple faults in the basin (Figure 1). Besides, the values of *HI*, |*AF*-50| and *Bs* in the basin are small. This is explained by the fact that the basin has undergone a long period of erosion and the overall uplift activity is not very intense. For *HI* values, we note that the basin has a lower *HI* value than sub-basins, suggesting that sub-basins are in the early stage of erosion evolution. According to the characteristics of erosion evolution of a basin, the response process of erosion activity to the tectonic uplift is in accordance with the propagation sequence of main

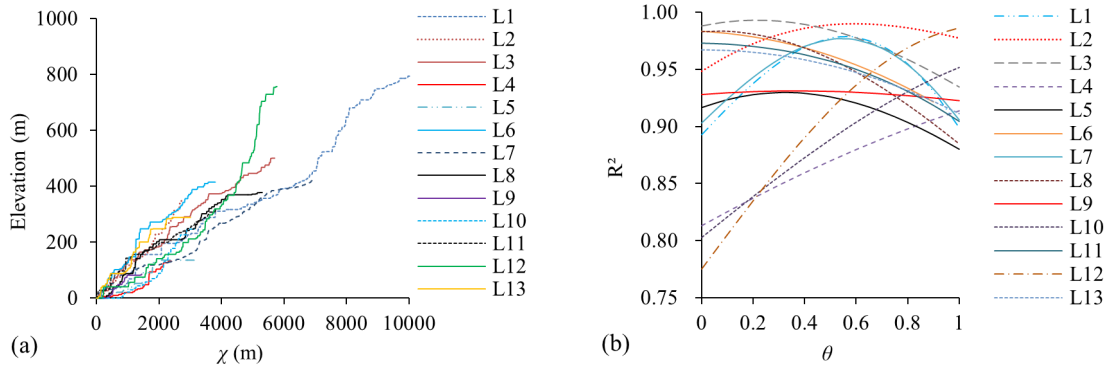

Figure 12 Steady-state analysis of longitudinal profiles. (a) Chi plot (χ-z) of the channels, transformed using Eqs. 3 and 4 with A_0=1 km² and average m/n=0.43, corresponding to the optimal fit; (b) R^2 as a function of θ for least-squares regression based on Eqs. 3 and 4.

channel-channel network-entire basin (Demoulin 2011). For the case of this basin, we believe that the erosion response of sub-basins to the erosion datum has just begun, but the erosion in the main channel has been going on for a long time. As the *HI* value of entire basin includes both sub-basins and the mainstream channel, while the *HI* value of sub-basin does not include the mainstream channel. Many reaches have large *SL*/*K* values (Figure 8), indicating that there are many steep segments within the basin, which is generally believed to account for the greater distribution of faults or knickpoints. These locations usually also have a considerable stream power value and lead to relatively strong erosion near their downstream reaches.

4 Conclusion

This study was the first to research the macroscopic geomorphic evolution of Buyuan Basin by analyzing its surface morphology, the coupling between longitudinal profiles and internal-external forces, and spatial changes of the hydrodynamic environment. Our major conclusions can be summarized as follows:

1) Some spatial differences in channel density exist in the basin, which are unrelated to tectonic activity and climate, and more likely influenced by lithology.

2) The tectonic activity of the basin, is generally not very strong, in that the relatively active region is equal to a medium-weak activity area. Moreover, *HI* is low, indicating that the macroscopic landform condition is not advantageous for promoting erosion and sediment yield.

3) The longitudinal profile of the mainstream channel is logarithmic. Under the condition of this, the upstream sediments generated by erosion are easily transported to the downstream channel and deposited, rather than being injected directly into the Lancang-Mekong River.

4) The annual average stream power in many reaches is less than 500 $W \cdot m^{-1}$ and the length accounts for 74% of the total length. The variation range of stream power in 50% of reaches is very limited, indicating that the hydrodynamic environment is relatively stable.

5) The longitudinal profiles of the main stream and most of its tributaries are considered to be unbalanced under the combined action of stream erosion and tectonic activity. The steepness index (k_{sn}) of longitudinal profile ranges from 22.01–45.58 with θ=0.43, revealing differential uplift in the basin.

Acknowledgements

We are very grateful to the two anonymous reviewers for their valuable advice. This study was financially supported by the National Key Research and Development Program of China (2016YFA0601601), the National Science and Technology Support Program (2013BAB06B03), the National Natural Science Foundation of China (41472155), Candidates of the Young and Middle-Aged Academic Leaders of Yunnan Province (2014HB005), and Program for Excellent Young Talents of Yunnan University.

References

Alekseevskii NI, Zavadskii AS, Krivushin MV, et al. (2015) Hydrological monitoring at international rivers and basins. Water Resources 42(6): 747-757. https://doi.org/10.1134/s0097807815060020

Altın TB (2012) Geomorphic signatures of active tectonic in drainage basins in the Southern Bolkar Mountain, Turkey. Journal of the Indian Society of Remote Sensing 40(2): 271-285. https://doi.org/10.1007/s12524-011-0145-8

Ambili V, Narayana AC (2014) Tectonic effects on the longitudinal profiles of the Chaliyar River and its tributaries, southwest India. Geomorphology 217: 37-47. https://doi.org/10.1016/j.geomorph.2014.04.013

Bernauer T (2002) Explaining success and failure in international river management. Aquatic Sciences 64(1): 1-19. https://doi.org/10.1007/s00027-002-8050-4

Chen CF, Fan ZM, Yue TX, et al. (2012) A robust estimator for the accuracy assessment of remote-sensing-derived DEMs. International Journal of Remote Sensing 33(8): 2482-2497. https://doi.org/10.1080/01431161.2011.615766

Chopra R, Dhiman RD, Sharma PK (2005) Morphometric analysis of sub-watersheds in Gurdaspur district, Punjab using remote sensing and GIS techniques. Journal of the Indian Society of Remote Sensing 33(4): 531-539. https://doi.org/10.1007/bf02990738

Dar RA, Romshoo SA, Chandra R, et al. (2014) Tectono-geomorphic study of the Karewa Basin of Kashmir Valley. Journal of Asian Earth Sciences 92: 143-156. https://doi.org/10.1016/j.jseaes.2014.06.018

Demoulin A (2011) Basin and river profile morphometry: A new index with a high potential for relative dating of tectonic uplift. Geomorphology 126(1-2): 97-107. https://doi.org/10.1016/j.geomorph.2010.10.033

Du QX, Han ZZ, Shen XL, et al. (2018) Zircon U–Pb geochronology and geochemistry of the post-collisional volcanic rocks in Eastern Xinjiang Province, NW China: implications for the tectonic evolution of the Junggar terrane. International Geology Review 60(3): 339-364. https://doi.org/10.1080/00206814.2017.1335243
Fan H, He DM, Wang HL (2015) Environmental consequences of damming the mainstream Lancang-Mekong River: A review. Earth-Science Reviews 146: 77-91. https://doi.org/10.1016/j.earscirev.2015.03.007
Gao MX, Zeilinger G, Xu XW, et al. (2016) Active tectonics evaluation from geomorphic indices for the central and the southern Longmenshan range on the Eastern Tibetan Plateau, China. Tectonics 35(8): 1812-1826. https://doi.org/10.1002/2015tc004080
Gao MX, Zeilinger G, Xu XW, et al. (2013) DEM and GIS analysis of geomorphic indices for evaluating recent uplift of the northeastern margin of the Tibetan Plateau, China. Geomorphology 190: 61-72. https://doi.org/10.1016/j.geomorph.2013.02.008
Gu ZK, Shi CX (2018) Dynamical characteristics of geomorphologic evolution of the basins covered by Pisha-sandstone in the Eastern wing of the Ordos Plateau, China. Journal of Mountain Science 15(5): 1046-1056. https://doi.org/10.1007/s11629-018-4859-8
Hack JT (1973) Stream-profiles analysis and stream-gradient index. Journal of Research of the U.S. Geological Survey 1(4): 421-429.
Hamdouni RE, Irigaray C, Fernández T, et al. (2008) Assessment of relative active tectonics, southwest border of the Sierra Nevada (southern Spain). Geomorphology 96(1): 150-173. https://doi.org/10.1016/j.geomorph.2007.08.004
He DM, Zhao WJ, Feng Y (2004) Research progress of international rivers in China. Journal of Geographical Sciences 14(S1): 21-28. (In Chinese) https://doi.org/10.1007/BF02841103
Hoke GD, Jing LZ, Hren MT, et al. (2014) Stable isotopes reveal high southeast Tibetan Plateau margin since the Paleogene. Earth and Planetary Science Letters 394: 270-278. https://doi.org/10.1016/j.epsl.2014.03.007
Li T, Wang H, Ma L, et al. (1982) The Geology of Asia. Geological Publishing House, Beijing. (In Chinese)
Li XP, Wang X, Chen S, et al. (2018) Petrology and zircon U–Pb dating of meta-calcsilicate from the Jiaobei terrane in the Jiao-Liao-Ji Belt of the North China Craton. Precambrian Research 313: 221-241. https://doi.org/10.1016/j.precamres.2018.04.018
Ma L (2002) Geological Atlas of China. Geological Publishing House, Beijing.
Mahmood SA, Gloaguen R (2012) Appraisal of active tectonics in Hindu Kush: Insights from DEM derived geomorphic indices and drainage analysis. Geoscience Frontiers 3(4): 407-428. https://doi.org/10.1016/j.gsf.2011.12.002
Ohmori H (1991) Change in the mathematical function type describing the longitudinal profile of a river through an evolutionary Process. Journal of Geology 99(1): 97-110. https://doi.org/10.1086/629476
Owono FM, Ntamak-Nida MJ, Dauteuil O, et al. (2016) Morphology and long-term landscape evolution of the South African Plateau in South Namibia. Catena 142: 47-65. https://doi.org/10.1016/j.catena.2016.02.012
Pérez-Peña JV, Azañón JM, Azor A, et al. (2009) Spatial analysis of stream power using GIS: SLk anomaly maps. Earth Surface Processes and Landforms 34(1): 16-25. https://doi.org/10.1002/esp.1684
Perron JT, Royden L (2013) An integral approach to bedrock river profile analysis. Earth Surface Processes and Landforms 38(6): 570-576. https://doi.org/10.1002/esp.3302
Pike RJ, Wilson SE (1971) Elevation-relief ratio, hypsometric integral, and geomorphic area-altitude analysis. Geological Society of America Bulletin 82(4): 1079. https://doi.org/10.1130/0016-7606(1971)82[1079:erhiag]2.0.co;2
Pipaud I, Loibl D, Lehmkuhl F (2015) Evaluation of TanDEM-X elevation data for geomorphological mapping and interpretation in high mountain environments — A case study from SE Tibet, China. Geomorphology 246: 232-254. https://doi.org/10.1016/j.geomorph.2015.06.025
Rabah M, El-Hattab A, Abdallah M (2017) Assessment of the most recent satellite based digital elevation models of Egypt. NRIAG Journal of Astronomy and Geophysics 6(2): 326-335. https://doi.org/10.1016/j.nrjag.2017.10.006
Rădoane M, Rădoane N, Dumitriu D (2003) Geomorphological evolution of longitudinal river profiles in the Carpathians. Geomorphology 50(4): 293-306. https://doi.org/10.1016/s0169-555x(02)00194-0
Seeber L, Gornitz V (1983) River profiles along the Himalayan arc as indicators of active tectonics. Tectonophysics 92(4): 335-367. https://doi.org/10.1016/0040-1951(83)90201-9
Shi CX, Shao WW (2014) Knickpoints within the Suoshui watershed and the implication for the age of sandstone pillars in Zhangjiajie, China. Geomorphology 221: 261-273. https://doi.org/10.1016/j.geomorph.2014.06.018
Singh O, Sarangi A, Sharma MC (2008) Hypsometric integral estimation methods and its relevance on erosion status of north-western Lesser Himalayan Watersheds. Water Resources Management 22(11): 1545-1560. https://doi.org/10.1007/s11269-008-9242-z
Stucki MD, Schlunegger F (2013) Identification of erosional mechanisms during past glaciations based on a bedrock surface model of the central European Alps. Earth and Planetary Sciences Letters 384: 57-70. https://doi.org/10.1016/j.epsl.2013.10.009
Summerfield MA (1991) Global Geomorphology. Singapore, Longman.
Wang YZ, Zhang HP, Zheng DW, et al. (2017) How a stationary knickpoint is sustained: New insights into the formation of the deep Yarlung Tsangpo Gorge. Geomorphology 285: 28-43. https://doi.org/10.1016/j.geomorph.2017.02.005
Whipple KX, Tucker GE (1999) Dynamics of the stream-power river incision model: Implications for height limits of mountain ranges, landscape response timescales, and research needs. Journal of Geophysical Research-Solid Earth 104(B8): 17661-17674. https://doi.org/10.1029/1999jb900120
Wu K, 2016. The Tectonic System and Genetic Mechanism Research of Simao Block in Yunnan Province. China University of Geosciences (Beijing), Beijing. (In Chinese)
Wu L, Xiao AC, Yang SF (2014) Impact of wind erosion on detecting active tectonics from geomorphic indexes in extremely arid areas: a case study from the Hero Range, Qaidam Basin, NW China. Geomorphology 224: 39-54. https://doi.org/10.1016/j.geomorph.2014.07.010
Wu W, Zhang S, Zhao S (2017) Analysis and comparison of SRTM1 DEM and ASTER GDEM V2 data. Journal of Geo-information Science 19(8): 1108-1115. (In Chinese with English abstract)
Zhang HY, Shi ZH, Fang NF, et al. (2015) Linking watershed geomorphic characteristics to sediment yield: Evidence from the Loess Plateau of China. Geomorphology 234: 19-27. https://doi.org/10.1016/j.geomorph.2015.01.014
Zhang JY, Jing LZ, Scherler D, et al. (2018) Spatiotemporal variation of late Quaternary river incision rates in southeast Tibet, constrained by dating fluvial terraces. Lithosphere 10(5):662-675. https://doi.org/10.1130/L686.1
Zhong RH, Yang CM, Fu KD, et al. (2011) Analysis of characteristics of water and sediment and their variability in Buyuan River Basin. Yangtze River 42(24): 29-33. (In Chinese with English abstract)